Article

Modeling gastric intestinal metaplasia in 3D organoids using nitrosoguanidine

Yuan Li^{1,2,3,†}, Jiena Chen^{4,†}, Tao Li², Jie Lin², Haocheng Zheng⁴, Nadia Johnson⁴, Xuebiao Yao^{5,*}, and Xia Ding^{2,3,4,*}

- National Institute of Traditional Chinese Medicine Constitution and Preventive Treatment of Diseases, Beijing University of Chinese Medicine, Beijing 100029, China
- ² School of Traditional Chinese Medicine, Beijing University of Chinese Medicine, Beijing 100029, China
- ³ Research Center for Spleen and Stomach Diseases of Traditional Chinese Medicine, Beijing University of Chinese Medicine, Beijing 100029, China
- $^{4}\,$ Dongzhimen Hospital, Beijing University of Chinese Medicine, Beijing 100700, China
- ⁵ MOE Key Laboratory of Cellular Dynamics, University of Science and Technology of China, Hefei 230027, China
- † These authors contributed equally to this work.
- * Correspondence to: Ding Xia, E-mail: dingx@bucm.edu.cn; Xuebiao Yao, E-mail: yaoxb@ustc.edu.cn

Edited by Hua Lu

Gastric intestinal metaplasia (GIM) represents a precancerous stage characterized by morphological and pathophysiological changes in the gastric mucosa, where gastric epithelial cells transform into a phenotype resembling that of intestinal cells. Previous studies have demonstrated that the intragastric administration of N-methyl-N'-nitro-N-nitrosoguanidine (MNNG) induces both gastric carcinoma and intestinal metaplasia in mice. Here, we show that MNNG induces GIM in three-dimensional (3D) mouse organoids. Our histological analyses reveal that MNNG-induced gastric organoids undergo classical morphological alterations, exhibiting a distinct up-regulation of CDX2 and MUC2, along with a down-regulation of ATP4B and MUC6. Importantly, metaplastic cells observed in MNNG-treated organoids originate from MIST1+ cells, indicating their gastric chief cell lineage. Functional analyses show that activation of the RAS signaling pathway drives MNNG-induced metaplasia in 3D organoids, mirroring the characteristics observed in human GIM. Consequently, modeling intestinal metaplasia using 3D organoids offers valuable insights into the molecular mechanisms and spatiotemporal dynamics of the gastric epithelial lineage during the development of intestinal metaplasia within the gastric mucosa. We conclude that the MNNG-induced metaplasia model utilizing 3D organoids provides a robust platform for developing preventive and therapeutic strategies to mitigate the risk of gastric cancer before precancerous lesions occur.

Keywords: gastric organoids, MNNG, intestinal metaplasia, trans-differentiation, precancerous lesion

Introduction

With over 1 million new cases each year, gastric cancer is ranked as the fifth most commonly diagnosed malignancy worldwide, and is a significant global health concern (Bray et al., 2018). In 2018, it was reported to be the third most common cause of cancer-related deaths, accounting for 784000 deaths worldwide (Smyth et al., 2020). The risk of gastric cancer involves interactions among *Helicobacter pylori* strain-specific

virulence factors, patient genotype, and environmental factors (Zhuo et al., 2019).

Perturbation of gastric acid secretion is an acute and chronic outcome of *H. pylori* infection that promotes gastric carcinogenesis (Wang et al., 2008; Yao and Smolka, 2019). The most common form of gastric cancer, the intestinal-type, is derived from chronic inflammation that progresses sequentially through several stages of pathological transformation, initially involving gland loss or atrophic gastritis and subsequently intestinal metaplasia, dysplasia, and adenocarcinoma (Correa, 1992). Gastric intestinal metaplasia (GIM), an established precursor lesion indicating increased susceptibility to gastric cancer, is characterized by the replacement of normal gastric mucosa with glands exhibiting an intestinal morphology (Correa et al., 2010), and has been shown to occur as a consequence of metaplastic

Received February 1, 2024. Revised July 18, 2024. Accepted August 16, 2024. © The Author(s) (2024). Published by Oxford University Press on behalf of *Journal of Molecular Cell Biology*, CEMCS, CAS.

This is an Open Access article distributed under the terms of the Creative Commons Attribution-NonCommercial License (https://creativecommons.org/licenses/by-nc/4.0/), which permits non-commercial re-use, distribution, and reproduction in any medium, provided the original work is properly cited. For commercial re-use, please contact journals.permissions@oup.com

trans-differentiation of chief cells into intestinal-like glandular structures (Mills and Goldenring, 2017). Intestinal metaplasia is classified as either the small intestinal/complete-type or the colonic/incomplete type, with the incomplete type being more likely to progress to adenocarcinoma (Krishnan et al., 2020).

Although cell culture models of human antral epithelial cells and normal gastric epithelial cells from biopsies have been developed for studying GIM (Ootani et al., 2000), these cell cultures cannot fully mimic the intricacies of the *in vivo* microenvironment. Thus, they may be insufficient for studying the complex crosstalk between different types of cells in the stomach. Compared to standard cell culture models, the mouse GIM model more closely resembles the pathology of human GIM; however, it is challenging to observe the sequential morphological changes in this system. In contrast, organoid culture allows for the observation of morphological evolution while replicating the stomach microenvironment, making it a widely used tool in gastric cancer research.

Previously, it has been shown that the DNA damage response, which modulates cell cycle progression and regulates a wide range of biological processes, is activated during the premalignant intestinal metaplasia stage (Olivieri et al., 2020). N-methyl-N'-nitro-N-nitrosoguanidine (MNNG), a widely used alkylating agent, has been positively evaluated as a potential treatment for epithelial injury by inducing DNA damage response pathways in the mouse model of gastric carcinogenesis (Jiao et al., 2014; Tang et al., 2020). However, how MNNG elicits GIM remains unclear.

Caudal-related homeobox transcription factor 2 (CDX2), a member of the homeobox gene family, is highly involved in the early intestinal differentiation of the intestinal epithelium. CDX2 activation can directly drive differentiation toward an intestinal phenotype (Barros et al., 2012). Interestingly, it has been demonstrated that the absence of CDX2 contributes to the transformation from intestinal stem cells to gastric stem cells in intestinal organoids (Simmini et al., 2014). MUC2, secreted by goblet cells in both the small and large intestine, is reported to be a direct target of CDX2 and is highly expressed in intestinal metaplasia (Mesquita et al., 2003; Mari et al., 2014). Despite reports on CDX2-induced intestinal metaplasia in gastric organoids and Cdx2-transgenic mouse models, exogenously derived CDX2 cannot recapitulate the change displayed by the native transcriptional network during the transition from a gastric transcriptional profile to an intestinal transcriptional profile. A more complete experimental model that fully reproduces the change in cell fate from a gastric identity to an intestinal one with the expression of endogenous CDX2 is essential (Ollivier et al., 2021; Koide et al., 2022).

In this study, we present a novel chemical approach to establish GIM organoids from murine gastric organoids using nitrosoguanidine. Our findings demonstrate that this method effectively maintains gastric organoids in a bipotential state, exhibiting both stomach- and intestinal-specific gene expression profiles and an enhanced potential for further gastric epithelial cell differentiation. Significantly, our study

delineated the rat sarcoma/B-raf proto-oncogene/extracellular signal-regulated kinase (RAS/BRAF/ERK) as a major participant in GIM development. This unique line of experimentation not only provides a valuable model for demonstrating gastric pathogenesis but also identifies hallmark events that underly the pathological evolution of gastric cancer and could inform screening methods for targeted therapeutics.

Results

MNNG treatment elicits CDX2 expression in MG-GOs

Gastric glands were obtained from C57BL/6J mice and cultured in Matrigel to generate gastric organoids (GOs) as described in our previous report (Figure 1A; Liu et al., 2020; Song et al., 2021). CDX2, a master regulator of the intestinal phenotype, possesses the ability to modulate DNA damage signaling, and enhance the survival of mammary cells in response to DNA damage (Johnson et al., 2018). Based on these findings, we aimed to assess the inducibility of CDX2 expression in MNNG-treated gastric organoids (MG-GOs) compared to the control group treated with DMSO (DM-GOs). Quantitative real-time polymerase chain reaction (qRT-PCR) analysis demonstrated no significant differences in Cdx2 mRNA expression levels between MG-GOs and DM-GOs up to 5 days after treatment. However, upon extending MNNG stimulation to 10 days, a marked increase in Cdx2 mRNA expression level was observed (Figure 1B). Immunofluorescence analysis showed that CDX2expressing organoids constituted 9.5% of the DM-GOs and 76.0% of the MG-GOs (Figure 1C-E; Supplementary Figure S1A). This indicated that differential expression of CDX2 was detected in GOs subjected to MNNG treatment on Day 10. Concurrently, F-actin labeled with phalloidin delineated the apical surface of cells and the luminal boundaries of organoids (Narayanan et al., 2023). Notably, F-actin was primarily localized to the apical-lateral membrane in DM-GOs, whereas in MG-GOs, phalloidin staining was also evident in the basolateral membrane, displaying aberrant adherens junctions in the epithelial barrier and suggesting alterations in epithelial cell adhesion. As shown in Figure 1F, cell polarity disruption was found in GOs treated with MNNG. Furthermore, DM-GOs predominantly exhibited a simple columnar epithelium, representative of healthy gastric mucosa, while MG-GOs displayed a more disorganized (pseudostratified and stratified) epithelium (Figure 1G and H). These findings appear to recapitulate the pseudo-stratification observed in gastric mucosal damage of patients with gastritis, which is indicative of reparative and protective changes in response to injurious insults (Aditi and Graham, 2012). SOX2 is a foregut marker that identifies progenitor cell populations in the stomach. SOX2-expressing organoids constituted 100.0% of the DM-GOs and 93.1% of the MG-GOs, showing significant downregulation in response to MNNG exposure (Figure 1I-K). However, the mRNA levels of Sox2 in GOs remained unchanged after MNNG stimulation (Supplementary Figure S1B and C). γ H2AX is a marker for DNA damage response and repair, specifically associated with double-strand breaks (Burma et al., 2001). Intriguingly, we observed an increase in yH2AX expression in

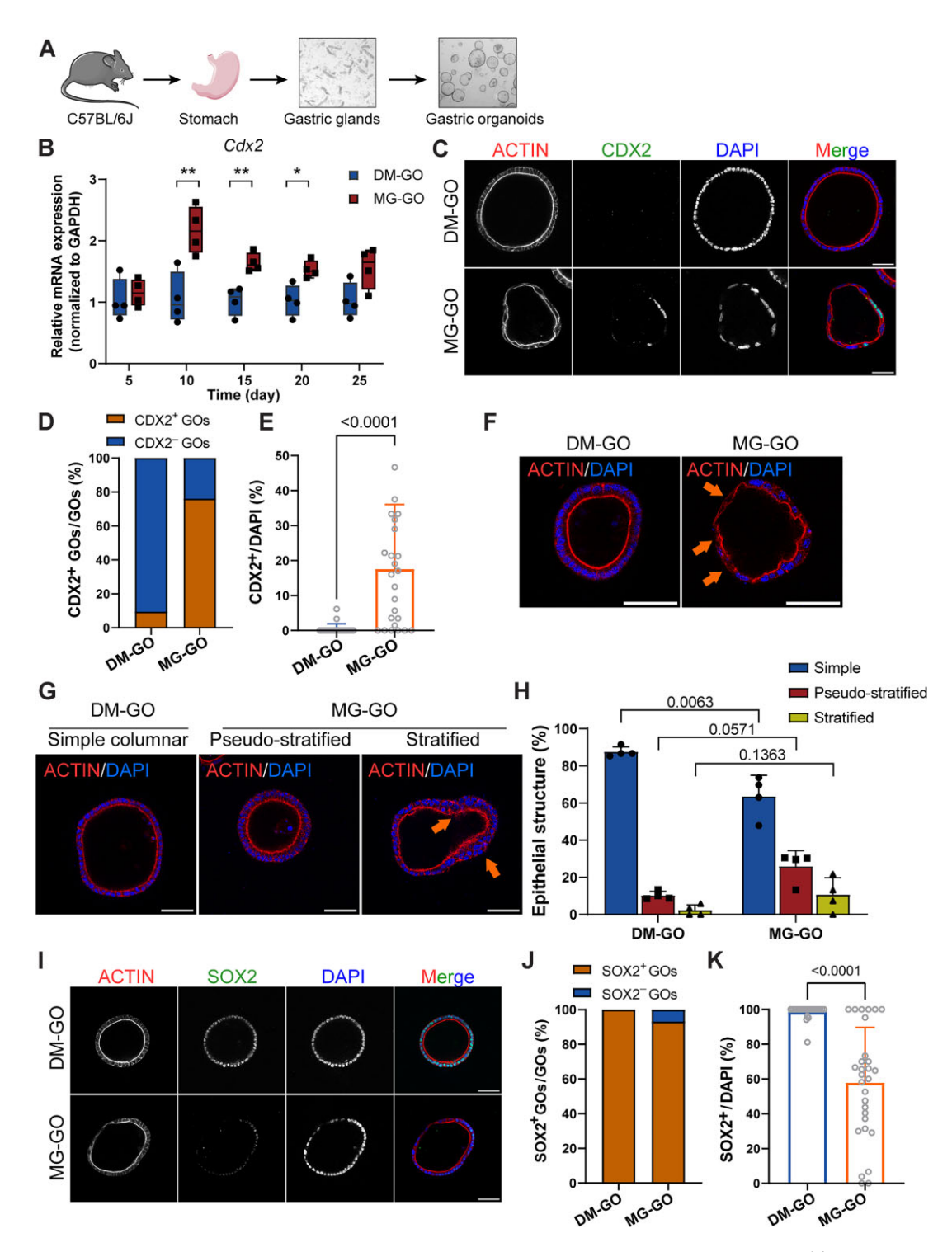


Figure 1 Nitrosoguanidine induction increases CDX2 expression and decreases SOX2 expression in MG-GOs. (A) Schematic representation of the GO culture establishment process. (B) Relative mRNA expression levels of Cdx2 on Days 5, 10, 15, 20, and 25 (n=4). Data represent mean \pm SEM. (C) Representative fluorescent images of CDX2 at Day 10. Scale bar, 50 μ m. (D) Stacked bar chart showing the proportion of CDX2-expressing organoids. (E) Percentage of CDX2+ cells in DM-GOs (n=21) and MG-GOs (n=25). Data represent mean \pm SEM. (F) Organoids stained with phalloidin and DAPI. Arrows indicate cell polarity disruption in MG-GO. Scale bar, 50 μ m. (G) Representative fluorescent images of epithelial structures in DM-GO and MG-GO. Arrows indicate stratified columnar epithelium in MG-GO. Scale bar, 50 μ m. (H) Summary of percentages of simple columnar, pseudostratified, and stratified epithelial structures in DM-GOs (n=114) and MG-GOs (n=121). (I) Representative fluorescent images of SOX2 at Day 10. Scale bar, 50 μ m. (J) Stacked bar chart showing the proportion of SOX2-expressing organoids. (K) Percentage of SOX2+ cells in DM-GOs (n=21) and MG-GOs (n=25). Data represent mean \pm SEM.

MG-GOs at the early stage of pathogenesis but a decrease at the stage concomitant with CDX2 expression (Supplementary Figure S1D-H), which suggests a reduction in DNA damage response signaling and a transition in cell fate. Collectively, these findings indicate that the suppression of DNA damage response signaling in gastric cells within MG-GOs facilitates their transformation into intestinal epithelial cells.

MNNG-induced MUC2 expression is a hallmark of GIM in MG-GOs

CDX2 expression in MG-GOs indicates the potential modeling of intestinal metaplasia in murine gastric organoids. Given that CDX2 regulates transcription of MUC2, a goblet cell marker, we subsequently assessed MUC2 expression in MG-GOs. qRT-PCR analysis indicated a significant increase in Muc2 mRNA expression levels in MG-GOs relative to DM-GOs on Day 15 (Figure 2A; Supplementary Figure S2A). Immunofluorescence revealed that on Day 15, MUC2⁺ cells were observed exclusively in MG-GOs, while DM-GOs did not contain MUC2+ cells (Figure 2B). MUC2expressing organoids accounted for 0.0% of DM-GOs and 66.7% of MG-GOs (Figure 2C and D; Supplementary Figure S2B). These observations emphasize the temporal dynamics of MUC2 expression, revealing a distinct maturation process induced by MNNG. Interestingly, we observed more irregular sphere shapes and rough edges in MG-GOs (Supplementary Figure S2C). To further analyze the morphological changes, histological examination was conducted using hematoxylin and eosin (H&E) staining. H&E staining of the organoids revealed distinct epithelial domains with an interior lumen (Figure 2E). In contrast to the MG-GOs, a more uniform pattern of cellular proliferation was observed throughout the columnar epithelium of DM-GOs. Importantly, the balloon-like appearance and size of goblet cells were noted in MG-GOs. Cells in MG-GOs appeared crowded, and goblet cells were often observed in association with evidence of immature differentiation, such as irregular mucin droplets of variable size within the cytoplasm (Correa et al., 2010). Additionally, it was observed that MG-GOs exhibited disrupted cell polarity. Alcian blue staining, which serves as an indicator of goblet-cell secretory function, demonstrated abundant acid muco-substance deposition in the apical region of cells as well as in the lumen of MG-GOs (Figure 2F), identifying a clear metaplastic process occurring within the intestinal phenotype. Furthermore, immunohistochemistry (IHC) staining for Ki67 revealed that regions of stratified epithelium in MG-GOs exhibited extensive and non-uniform epithelial proliferation with a broader distribution (Figure 2G). Slightly higher rates of cell proliferation, assessed by EdU staining, were shown in MG-GOs during intestinal metaplasia, consistent with findings from several prior studies (Figure 2H and I; Wang et al., 2011; Shimizu et al., 2016). Specifically, organoids treated with MNNG for 15 days showed a higher proportion of EdU+ cells compared to those treated for only 5 days (Figure 2); Supplementary Figure S2D and E), indicating that MNNG induces early-stage proliferation arrest through activation of the DNA

damage response, evidenced by increased $\gamma H2AX$ expression. The concurrent upregulation of CDX2 after MNNG administration triggers other critical cellular responses, including activation of DNA repair pathways, thereby facilitating damage resolution. These molecular events are associated with the formation of GIM in MG-GOs.

MG-GOs exhibit parietal cell loss and impaired gastric acid secretion

To assess the maintenance of parietal cells under MNNG stimulation in gastric organoids, we examined the expression of the proton pump ATP4B using immunofluorescence. As shown in Figure 3A-C, ATP4B-expressing organoids accounted for 75.0% of the DM-GOs and 36.0% of the MG-GOs, indicating downregulation of ATP4B expression under MNNG stimulation. This finding was supported by western blot and qRT-PCR analysis (Figure 3D and E). To further investigate whether the parietal cells in MG-GOs were capable of acid secretion in response to histamine, we employed acridine orange, a fluorescent dye known to exhibit green fluorescence at neutral pH and shift to red when accumulated in acidic organelles, such as the secretory canaliculus of parietal cells (Lambrecht et al., 2005). Remarkably, upon the addition of histamine (100 µM) to the MG-GOs, acridine orange accumulated in cell vesicles, accompanied by a decreased red-to-green fluorescence ratio (Figure 3F and G). This suggests that MNNG treatment suppressed acid secretion from parietal cells in the gastric organoids, indicating similarities between murine-derived metaplastic organoids induced by MNNG and organoids derived from clinical patients (Supplementary Figure S3C). Collectively, these results indicate a marked alteration of parietal cell physiology within gastric organoids treated with MNNG, including impaired gastric acid secretion.

MIST1⁺ cells give rise to CDX2⁺ metaplastic cells in MG-GOs

It has been previously established that isthmus stem cells serve as the origin of metaplasia in the gastric corpus (Hayakawa et al., 2017). To test the hypothesis that CDX2-expressing metaplastic cells were derived from isthmus stem cells in our models, we first assessed MIST1, a marker of quiescent stem cells in the gastric corpus isthmus (Hayakawa et al., 2015). MIST1 expression was observed in 45.2% of cells in DM-GOs and 26.3% of cells in MG-GOs (Figure 4A and B). The expression pattern of *Mist1* was further validated by qRT-PCR analysis (Figure 4C). Compared to DM-GOs, MG-GOs had fewer GSII+MIST1+ cells (Figure 4D and E) but more EdU+MIST1+ cells (Figure 4F-H). The reduced proportion of GSII+MIST1+ cells suggested a decrease in foveolar cells among MIST1-expressing cells in MG-GOs. The higher proportion of EdU⁺ cells indicated increased cell proliferation among MIST1-expressing stem cells in MG-GOs. Notably, CDX2⁺ cells were observed within the population of MIST1-expressing cells in MG-GOs on Day 10 (Figure 4I), indicating the trans-differentiation of MIST1⁺ cells into CDX2⁺ metaplastic cells following MNNG treatment. Moreover, MIST1+

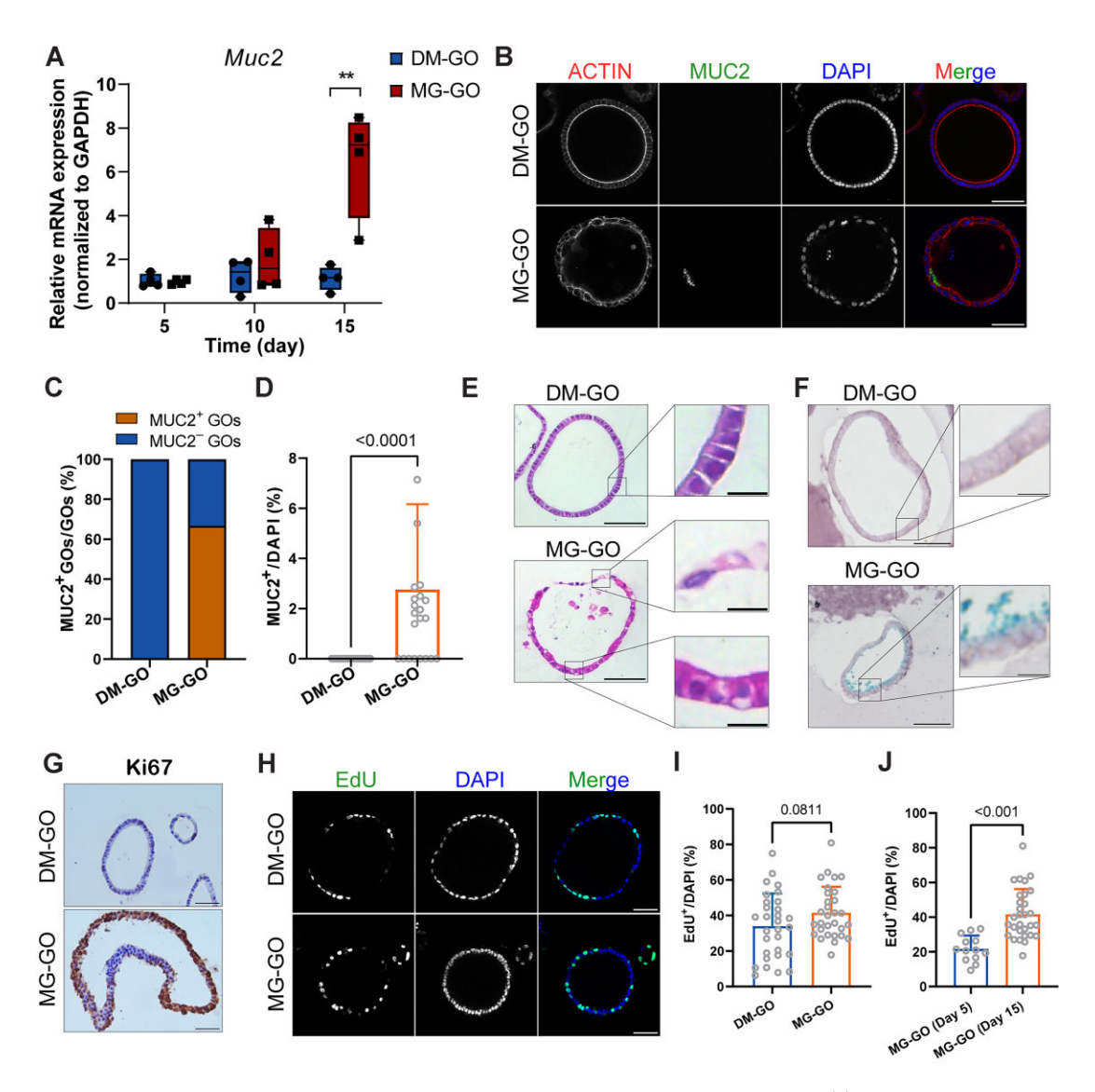


Figure 2 Nitrosoguanidine induction triggers MUC2 expression and GIM characteristics in MG-GOs. (**A**) Relative mRNA expression levels of $\mathit{Muc2}$ at Days 5, 10, and 15 ($\mathit{n}=4$, mean \pm SEM). (**B**) Representative fluorescent images of MUC2 at Day 15. Scale bar, 50 μm. (**C**) Stacked bar chart showing the proportion of MUC2-expressing organoids. (**D**) Percentage of MUC2⁺ cells in DM-GOs ($\mathit{n}=23$) and MG-GOs ($\mathit{n}=24$). Data represent mean \pm SEM. (**E** and **F**) Representative images of H&E staining and alcian blue staining for DM-GOs and MG-GOs. Scale bar, 50 μm (lower magnification) and 10 μm (higher magnification). (**G**) Representative images of Ki67 staining for DM-GOs and MG-GOs. Scale bar, 50 μm. (**H**) Representative images of EdU staining for DM-GOs and MG-GOs. Scale bar, 50 μm. (**I**) Percentage of EdU⁺ cells in DM-GOs and MG-GOs ($\mathit{n}=30$) each group, mean \pm SEM). (**J**) Percentage of EdU⁺ cells in MG-GOs on Days 5 and 15 (mean \pm SEM).

cells persisted in the GO cultures for 60 days, confirming the stability of the gastric phenotype (Supplementary Figure S4A). To assess the potential progression of the MG-GOs toward gastric carcinoma, we examined CD44 and c-MYC expression in GOs cultured for 60 days. Subsequent analysis showed that MNNG treatment led to increased expression of CD44 and c-MYC in the organoids, suggesting malignant transformation within MG-GOs (Supplementary Figure S4B and C). Consequently, our results indicate that metaplastic cell trans-differentiation in gastric organoids in response to chronic damage arises from MIST1-expressing cells.

Bulk RNA-sequencing reveals GIM signatures in MG-GOs

Bulk RNA-sequencing (RNA-seq) was employed to investigate the molecular characteristics of DM-GOs and MG-GOs (Figure 5A). Principal component analysis (PCA) and hierarchical clustering were used to compare the molecular characteristics of the two organoid groups, aiming to delineate similarities and differences between intestinal metaplasia and normal gastric development (Figure 5B; Supplementary Figure S5A). Subsequently, differential gene expression analysis between the MG-GOs and DM-GOs was visualized using a volcano plot (log2(fold change) > 1, P < 0.05; Supplementary Figure S5B).

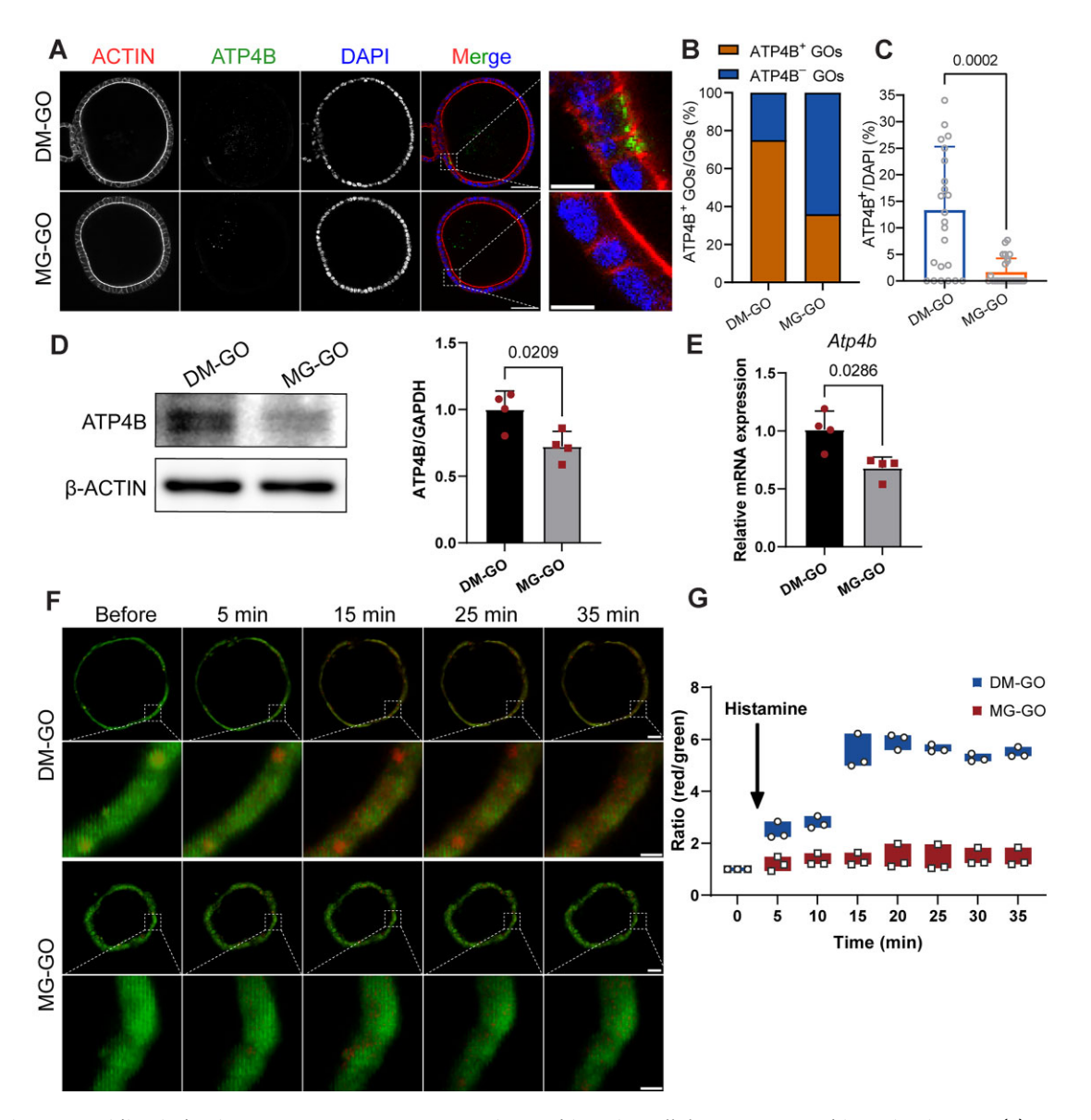


Figure 3 Nitrosoguanidine induction suppresses ATP4B expression and impairs cellular response to histamine in GOs. (A) Representative fluorescent images of ATP4B at Day 5. Scale bar, 50 μ m (lower magnification) and 10 μ m (higher magnification). (B) Stacked bar chart showing the proportion of ATP4B-expressing organoids. (C) Percentage of ATP4B+ cells in DM-GOs (n=24) and MG-GOs (n=25). Data represent mean \pm SEM. (D) Relative protein expression levels of ATP4B in MG-GOs compared to DM-GOs (n=4, mean \pm SEM). (E) Relative mRNA expression levels of Atp4b in MG-GOs compared to DM-GOs (n=4, mean \pm SEM). (F) Acridine orange staining before and after histamine (100 μ M) treatment. Scale bar, 50 μ m (lower magnification) and 10 μ m (higher magnification). (G) Quantification of red/green (600–650 nm/500–550 nm) ratio changes in response to histamine from three individual regions of interest.

Heatmaps highlighted upregulation of intestinal-associated genes and downregulation of gastric-associated genes in MG-GOs (Supplementary Figure S5C), defining an intestinal signature. To validate the transcriptomic features of intestinal metaplasia, we compared the gastric and intestinal gene signatures of the organoids using previously reported gene lists (Owen et al., 2018). Correlation analysis revealed that MNNG stimulation upregulated intestinal gene expression and downregulated stomach-specific transcripts in the GOs (Figure 5C; Supplementary Figure S5D).

Gene Ontology analysis and gene set enrichment analysis (GSEA) revealed that MG-GOs at a more advanced stage of progression showed upregulation of genes involved in the morphogenesis of an epithelial bud, intestinal epithelial cell differentiation, extracellular matrix structural constituent, cell adhesion, and epithelial to mesenchymal transition (Figure 5D). To further elucidate which subtypes of intestinal metaplasia MG-GO corresponds to, we compared our transcriptional profiling of the MG-GOs with the gastrointestinal metaplasia derived from patients (Companioni et al., 2017). We found that genes that

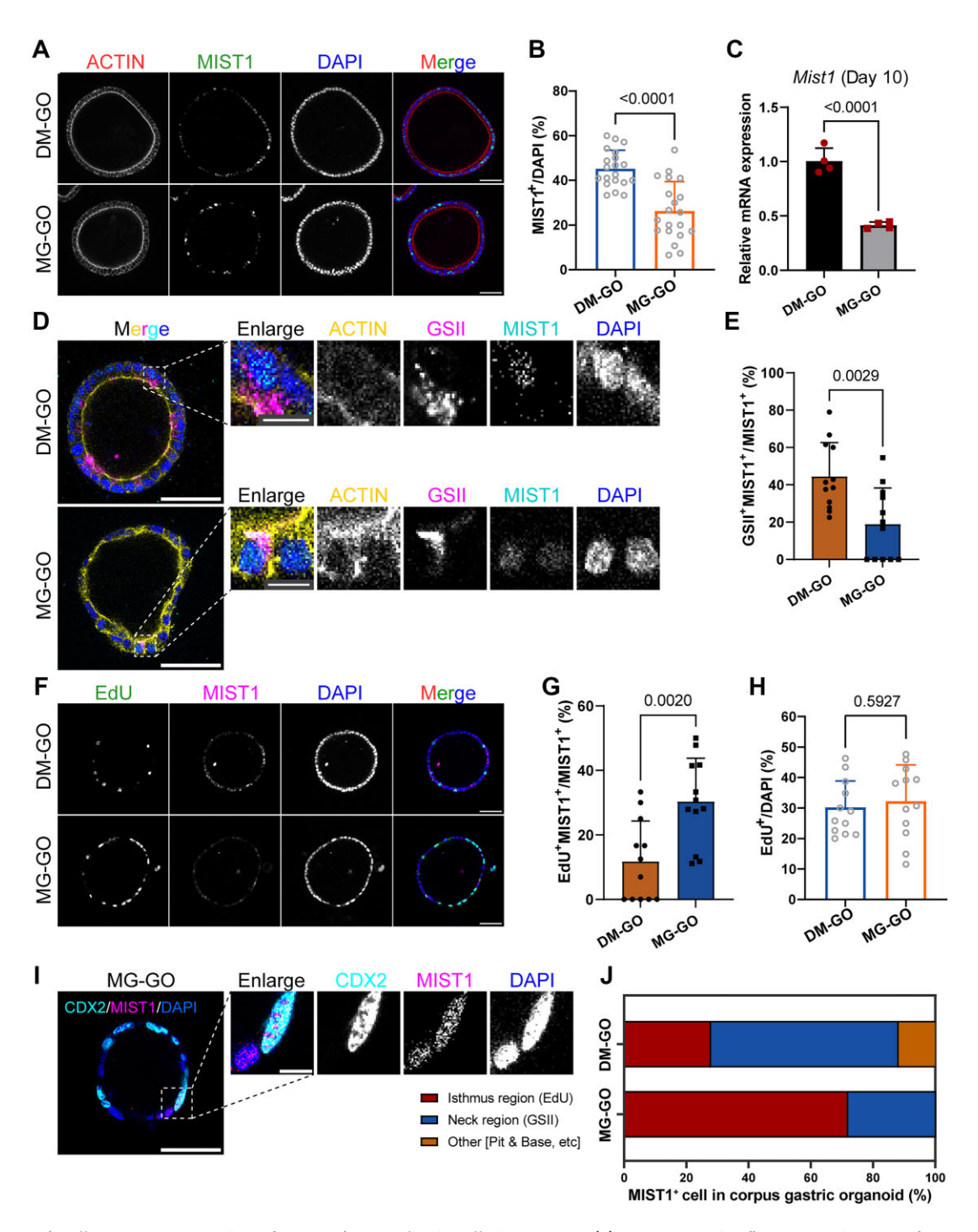


Figure 4 MIST1+ cells serve as progenitors for CDX2+ metaplastic cells in MG-GOs. (**A**) Representative fluorescent images of MIST1 at Day 10. Scale bar, 50 μ m. (**B**) Percentage of MIST1+ cells in DM-GOs (n=20) and MG-GOs (n=20). Data represent mean \pm SEM. (**C**) Relative mRNA expression levels of *Mist1* on Day 10 (n=4, mean \pm SEM). (**D**) Representative fluorescent images of GSII and MIST1 at Day 10. Scale bar, 50 μ m (lower magnification) and 10 μ m (higher magnification). (**E**) Percentage of GSII+MIST1+ epithelial cells among total MIST1+ epithelial cells in DM-GOs (n=12) and MG-GOs (n=12). Data represent mean \pm SEM. (**F**) Representative images of EdU and MIST1 at Day 10. Scale bar, 50 μ m. (**G**) Percentage of EdU+MIST1+ epithelial cells among total MIST1+ epithelial cells in DM-GOs (n=12) and MG-GOs (n=12). (**H**) Percentage of EdU+ cells in DM-GOs (n=12) and MG-GOs (n=12). (I) Representative fluorescent images of CDX2 and MIST1 in MG-GOs at Day 10. Scale bar, 50 μ m (lower magnification) and 10 μ m (higher magnification). (J) Stacked bar chart showing the distribution of MIST+ cells in corpus gastric organoids, categorized by their location per total MIST+ cells.

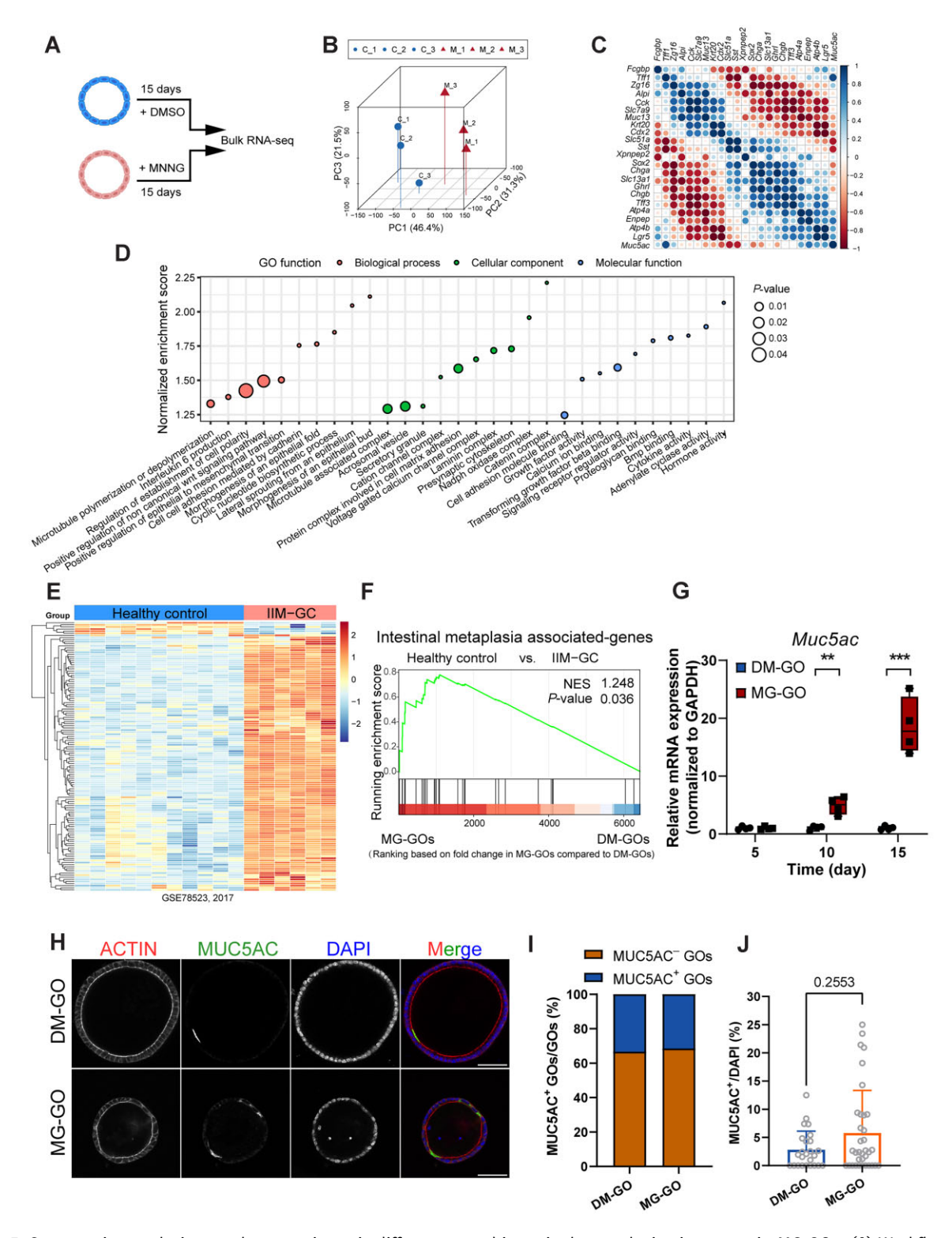


Figure 5 Comparative analysis reveals transcriptomic differences and intestinal metaplasia signatures in MG-GOs. (**A**) Workflow depicting RNA-seq analysis. (**B**) 3D PCA of DM-GOs and MG-GOs. (**C**) Spearman correlation matrix of gastric and intestinal signature genes clustered using corrplot Bioconductor. (**D**) GSEA and Gene Ontology analysis of DEGs between DM-GOs and MG-GOs, visualized as a dot plot of significantly enriched terms. (**E**) Heatmap displaying DEGs between healthy gastric mucosa and IIM-GC. (**F**) GSEA of genes upregulated in IIM-GC compared to healthy gastric mucosa, showing similarity to IIM-GC. (**G**) Relative mRNA expression levels of Muc5ac at Days 5, 10, and 15 (n = 4, mean \pm SEM). (**H**) Representative fluorescent images of MUC5AC at Day 15. (**I**) Stacked bar chart showing the proportion of MUC5AC-expressing organoids. (**J**) Percentage of MUC5AC⁺ cells in DM-GOs (n = 25) and MG-GOs (n = 35). Data represent mean \pm SEM.

were upregulated in MG-GOs were also highly enriched among the upregulated genes in human incomplete intestinal metaplasia (IIM) subtypes that can progress to gastric cancer (IIM-GC) (Figure 5E and F; Supplementary Figure S6A-F). There is considerable evidence suggesting that SOX2 is not only expressed in normal gastric mucosa, mainly in the presumptive stem cell compartment, but also maintained in incomplete (MUC5AC+) intestinal metaplasia subtypes (Gonzalez et al., 2013; Camilo et al., 2015).

Immunofluorescence staining showed that SOX2 was still expressed in MG-GOs, albeit at a reduced level compared to the DM-GOs (Supplementary Figure S6G). The MG-GOs were strongly positive for MUC5AC, a gastric foveolar cell marker, but lost MUC6 expression (Figure 5H–J; Supplementary Figure S6I–K). Similar changes in *Muc5ac* and *Muc6* mRNA expression levels were confirmed by qRT-PCR analysis (Figure 5G; Supplementary Figure S6H), suggesting that mucin expression in MG-GOs was consistent with clinically observed IIM. Therefore, our model system successfully recapitulated significant aspects of IIM observed in clinical settings.

The RAS/ERK signaling pathway plays a role in intestinal metaplasia formation

The similarity between the intestinal metaplasia model, induced by CDX2 overexpression in GOs derived from pluripotent stem cells (Johnson et al., 2018), and the presented MG-GOs, reinforces our previous findings and provides further evidence for CDX2's crucial role in intestinal metaplasia (Supplementary Figure S7A and B). Based on this, we conducted correlation analysis of CDX2 expression in MG-GOs. GSEA analysis revealed enrichment of RAS signaling pathways, including 'RHO GTPase effectors', 'Regulation of RAS by GAPs', and 'RHO GTPases activate Formins', among targets strongly associated with CDX2 in MG-GOs (Supplementary Figure S7C). This aligns with prior research (Zhu et al., 2014), showing that systemic KRAS activation can induce GIM (Matkar et al., 2011). ERK1/2 signaling pathway activation due to RAS mutation is linked with the progression of GIM to gastric cancer (Higashi et al., 2004; Fujiwara-Tani et al., 2021; Zhu et al., 2021). Despite extensive research, it remains uncertain whether the RAS/ERK pathways are activated and coordinate cell-fate decisions in response to GIM formation. We used two unbiased approaches to investigate the mechanisms underlying GIM in MG-GOs, performing GSEA comparing IIM-GC from patient samples with MG-GOs, and evaluating the expression of the RAS/ERK signaling pathway in MG-GOs. GSEA revealed that transcriptional changes in a more advanced stage of pathogenesis following treatment with MNNG correlated highly with those of IIM-GC (Figure 6A), suggesting that a common set of RAS signaling pathways may respond to the onset of GIM. To ascertain the critical role of the RAS pathway in GIM, we utilized MRTX1133, a potent and selective KRAS^{G12D} inhibitor (Hallin et al., 2022). MG-GOs treated with MRTX1133 exhibited a significant reduction in size and a lower proportion of EdU⁺ cells compared to untreated MG-GOs (Figure 6B). Collectively, these results suggest that MRTX1133 inhibits the growth of metaplastic organoids. Subsequently, we examined the expression pattern of RAS signaling in MG-GOs. Immunofluorescence analysis revealed higher RAS levels in MG-GOs compared to the DM-GOs, while the RAS signal was inhibited in MRTX1133-treated MG-GOs (Figure 6C). Furthermore, the MG-GOs showed elevated ERK1/2 and p-ERK1/2 levels compared to the DM-GOs, and phosphorylation was significantly reduced with MRTX1133 treatment (Figure 6D; Supplementary Figure S8). BRAF, a member of the RAF family and downstream to RAS in the signaling pathway, was sporadically observed in MG-GOs, but not in DM-GOs or MRTX1133-treated MG-GOs, consistent with prior findings (Figure 6E; Lee et al., 2003). These observations suggest that MG-GOs with activated RAS/BRAF/ERK signaling may undergo accelerated progression of GIM. RAS expression was also detected in a distinct subset of MIST1+ cells within MG-GOs (Figure 6F). We found that RAS+MIST1+ cells were encircled by adjacent cells expressing RAS. Thus, we speculate that MNNG induction promotes activated RAS in MIST1⁺ cells, initiating a complete spectrum of metaplastic lineage transitions.

Discussion

GIM arises from chronic injury and the aberrant regenerative processes underlying the pathogenesis of gastric cancer. However, the molecular network linking chronic damage and aberrant regeneration to lesion formation, as well as the cellular origin of these lesions, remains largely unknown. It has been reported that GIM may exhibit phenotypic plasticity that is triggered by the expression of CDX2, a transcription factor maintaining intestinal differentiation in the gastrointestinal tract (Francis et al., 2019). However, these studies were cross-sectional, assessing biopsies at only a single time point (Park et al., 2010; Barros et al., 2012). Here, we aimed to characterize GIM development and establish a model of intestinal metaplasia, showing that continuous MNNG exposure increased CDX2 expression and downstream intestinal-specific markers in GOs.

Upon MNNG exposure, gastric organoids activate a DNA damage response with serine phosphorylation of H2AX (γ H2AX), initially sensing DNA breaks and leading to temporary proliferation arrest to accommodate DNA damage repair. Recently, CDX2 was found to function independently of transcription, serving as a DNA damage inhibitor and enhancing cell survival under DNA-damaging conditions (Johnson et al., 2018).

Analyzing CDX2 expression every 5 days during MNNG administration revealed its pivotal role in driving GIM formation. CDX2 mRNA and protein expression emerged in the GOs on Day 10 following initiation of MNNG treatment and persisted throughout continuous induction, consistent with its ability to enhance cell survival under conditions that contribute to DNA damage (Rubin et al., 2007). A reduction in γ H2AX signaling on Day 10 suggests attenuation of DNA damage response signaling, a phenomenon that is conserved in differentiating cells (Vermezovic et al., 2012).

Simultaneously, a profound reduction in SOX2 protein levels after 10 days following MNNG exposure, along with a corresponding decline in mRNA by Day 20, suggests reduced SOX2

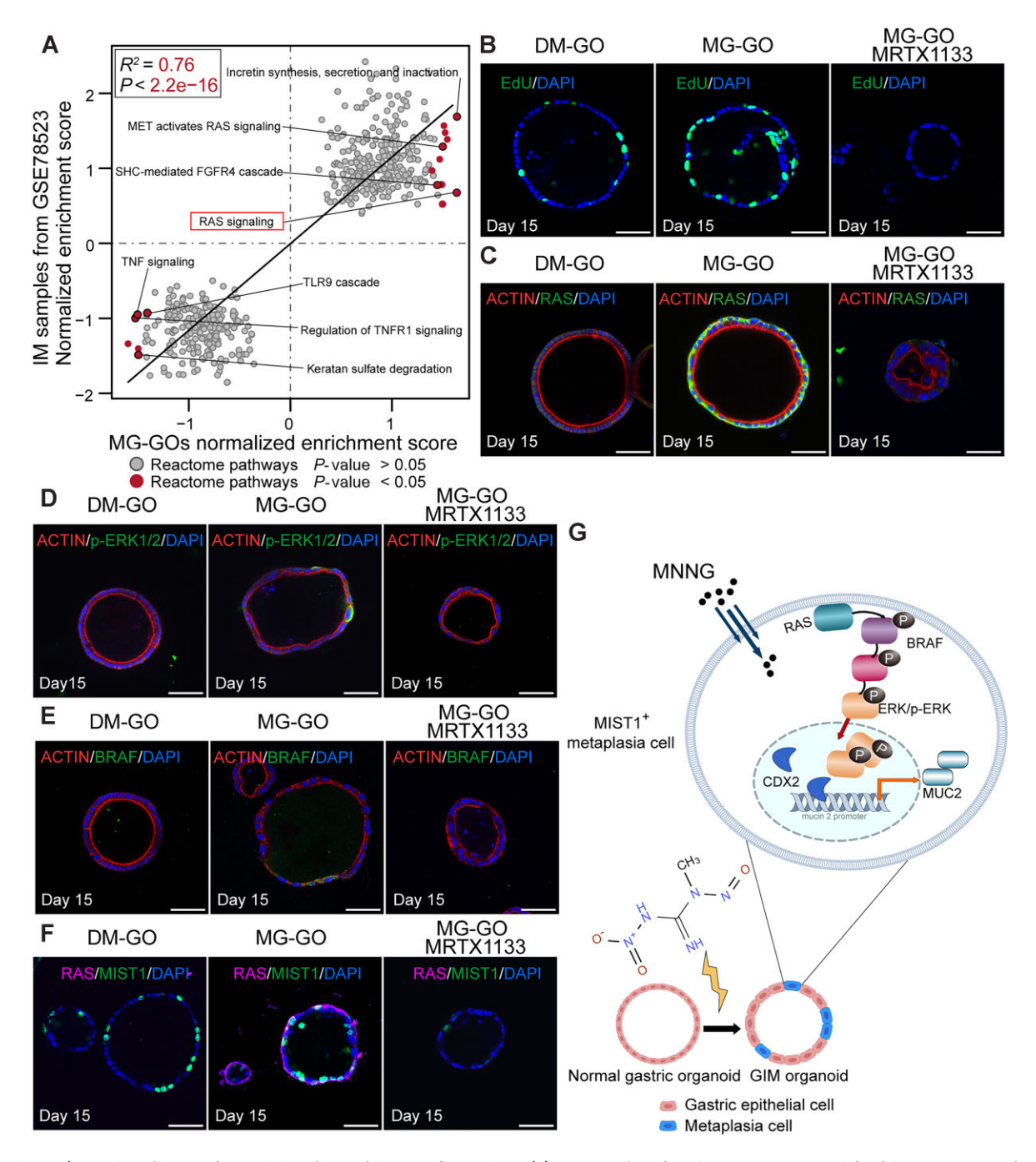


Figure 6 RAS/ERK signaling pathway is implicated in GIM formation. (**A**) Scatterplot showing gene sets enriched in MG-GOs and IIM-GC. IM, intestinal metaplasia. (**B**) Representative images of EdU staining for DM-GOs, MG-GOs, and MG-GOs treated with MRTX1133 on Day 15. Scale bar, 50 μ m. (**C**) Immunofluorescent staining of RAS in DM-GOs, MG-GOs, and MG-GOs treated with MRTX1133. Scale bar, 50 μ m. (**D**) Immunofluorescent staining of phosphorylated ERK1/2 (p-ERK1/2) in DM-GOs, MG-GOs, and MG-GOs treated with MRTX1133. Scale bar, 50 μ m. (**E**) Immunofluorescent staining of BRAF in gastric organoids. Scale bar, 50 μ m. (**F**) Organoids stained with EdU, anti-RAS, and DAPI. Scale bar, 50 μ m. (**G**) Schematic illustration of the proposed molecular mechanism underlying changes in MG-GOs during GIM.

involvement in GIM (Camilo et al., 2015). However, little is known about the mechanisms whereby MNNG downregulates SOX2 protein levels without a synchronous decrease in mRNA levels.

Consistent with the progressive loss of parietal cells in gastric carcinogenesis, we observed a reduction in parietal cells and impaired gastric acid secretion in MG-GOs on Day 5. Interestingly, changes in cellular polarity were observed following the induction of differential CDX2 expression in MG-GOs by Day 10. F-actin was shown to be randomly distributed within MG-GOs and was evenly present in all regions of the organoids, while in DM-GOs, F-actin was restricted to the apical plasma membrane. Polarity changes in MG-GOs indicate disrupted tight junction balance, revealing compromised epithelial barrier integrity and secretory activity (Fatehullah et al., 2013; Bhat et al., 2018). Early intestinal differentiation precedes morphological changes, such as the appearance of goblet cells, indicating an intermediate stage in the shift of GOs toward intestinal metaplasia (Niwa et al., 2005).

Previous reports suggest that mature chief cells secreting zymogens in the stomach corpus mucosa are the origin of metaplastic cells (Mills and Goldenring, 2017; Caldwell et al., 2022). In our study, MIST1-expressing cells in MG-GOs underwent the trans-differentiation, giving rise to CDX2+ metaplastic cells and revealing cellular plasticity during GIM formation. Epstein–Barr virus (EBV), an oncogenic herpesvirus associated with gastric cancers of lymphocytic and epithelial origin, has been implicated in EBNA1-induced chromosome instability (Li et al., 2023). Further comparative analysis of mechanisms underlying GIM induction by MNNG, chemokines, and EBV using the three-dimensional (3D) GO model established in this work would be highly valuable.

CDX2 binds to the MUC2 promoter, activating MUC2 translation and expression (Mesquita et al., 2003; Yamamoto et al., 2003; Mari et al., 2014). Importantly, we observed a significant increase in MUC2 mRNA levels in MG-GOs, accompanied by MUC2 staining in goblet cells on Day 15. This coordinated upregulation of CDX2 and MUC2 expression in MG-GOs suggests an initial process of intestinal differentiation, as DM-GOs do not exhibit significant amounts of CDX2 and MUC2. These observations indicate a close relationship between MNNG and GIM. H&E staining of serial sections, as well as alcian blue staining, showed goblet cells in MG-GOs but not in DM-GOs. Disorganized epithelium and high Ki67 expression in MG-GOs are consistent with the greater stratification observed in the gastric mucosa of patients with GIM, possibly due to chronic trauma-induced regeneration (Graham et al., 2019). Additionally, we observed increased expression of MUC5AC and decreased expression of MUC6 in MG-GOs. The increase in MUC5AC expression in MG-GO cells suggests the retention of a gastric phenotype characterized by superficial epithelium features, even during the process of GIM formation (Babu et al., 2006). This expression pattern aligns with observations of IIM. Our RNA-seq results also reveal an expression pattern similar to those of clinical samples, validating the involvement of RAS signaling cascade activation

in GIM. Considering the underlying mechanisms of gastric carcinogenesis, we assessed the effects of the drug MRTX1133, a potent, selective, and non-covalent KRAS^{G12D} inhibitor, in MG-GOs, elucidating the role of the RAS signaling pathway in precancerous gastric lesions.

In summary, the MG-GO model delineates the molecular network underlying GIM and gastric cancer development. Our findings provide insights into the mechanisms involved in MNNG-induced trans-differentiation of the gastric mucosa *ex vivo*. Overall, MNNG-induced GIM using organoid technology may aid in dissecting the molecular mechanisms of GIM and discovering novel strategies for targeted therapies to address unmet medical needs. Moreover, repurposing MRTX1133 may offer a significant therapeutic opportunity to reprogram the gastric mucosa in patients with gastric precancerous lesions.

Materials and methods

Gastric organoid culture

Gastric organoids were cultured as previously described and passaged every 5 days with a split ratio of 1:3-1:4 (Bartfeld et al., 2015). Treatment with MNNG was performed after stable culture for two passages. C57BL/6J mice (aged 6-8 weeks) were used for corpus gastric organoid cultures. All animal experiments were approved by the ethics committee of the Beijing University of Chinese Medicine and were conducted in accordance with the committee's guidelines. Animals were euthanized via carbon dioxide inhalation followed by cervical dislocation before stomach removal and washing with ice-cold Dulbecco's phosphate-buffered saline (DPBS), followed by removing fat and connective tissue. Subsequently, the stomach was incubated in 5 mM EDTA (Sigma) in DPBS at 4°C in a shaking incubator. After 2 h, the stomach was placed into 5 ml dissociation buffer (43.4 mM sucrose, 54.9 mM D-sorbitol in DPBS), and shaken vigorously for 1 min by hand to dissociate individual glands from the tissue to obtain the desired gland concentration. The medium containing dissociated glands was centrifuged at 4°C, and $300 \times g$ for 5 min and resuspended in Matrigel (Corning). The suspended glands in Matrigel were added to 24-well culture plates (50 µl Matrigel per well) or 8-chamber slides (for imaging). After Matrigel polymerization at 37°C, gastric organoid growth medium consisting of advanced DMEM/F12 plus 100 ng/ml Wnt3a, 500 ng/ml R-spondin (R&D), 10 nM Gastrin (R&D), 1 mM N-acetylcysteine (Sigma-Aldrich), 100 ng/ml FGF10 (R&D), 100 ng/ml Noggin (R&D) and 10 nM Y-27632 (Sigma-Aldrich) the latter being applied during the initial 4 days only, was added to wells and replaced every 3 days. MRTX1133 (HY-134813, MCE) was dissolved in DMSO. Treatment with MRTX1133 was administered to MG-GOs for a duration of 24 h at a concentration of 100 nM.

To establish human intestinal metaplasia organoids, fresh tissue samples were obtained from patients with GIM who underwent curative gastrectomy at Dongzhimen Hospital (Supplementary Figure S3A). Organoid lines were established as described in our previous study (Bartfeld et al., 2015).

Approximately 1 cm long mucosa strips were excised from the GIM samples towards the adjacent non-pathological region in the direction of the corpus. Each tissue piece was divided into two pieces for pathological examination and establishment of organoids (Supplementary Figure S3B).

Ouantitative real-time PCR

Total RNA was isolated from organoids, and cDNA was synthesized (Vazyme) and analyzed by real-time PCR (SYBR, Vazyme) on CFX96 Touch System (Bio-Rad). The detailed sequences of the primers that were used are listed in Supplementary Table S2.

Antibodies

Ki67 (Abcam, ab16667, 1:250), γH2AX (phospho S139) (Cell Signaling Technology, CST9718, 1:400), ATP4B (Abcam, ab2866, 1:2000), CDX2 (Abcam, ab76541, 1:50), SOX2 (Abcam, ab92494, 1:50), MUC5AC (Abcam, ab3649, 1:100), MUC6 (Abcam, ab192318, 1:100), MUC2 (Santa Cruz, sc-7314, 1:100), Ras (Cell Signaling Technology, CST91054, 1:600), Erk1/2 (Cell Signaling Technology, CST4695, 1:600), p-Erk1/2 (Cell Signaling Technology, CST4370, 1:300), CD44 (Proteintech, 60224-1-Ig, 1:250), and c-MYC (Proteintech, 10828-1-AP, 1:450) were obtained commercially.

Immunofluorescence

Organoids were fixed with 4% paraformaldehyde for 20 min at room temperature, followed by tissue permeabilization with 0.2% Triton X-100 in PBS for 20 min, and then blocked in 1% BSA in PBS. Primary antibodies were incubated overnight at 4°C. Next, the organoids were incubated with Alexa Flour 488 or 647 (Jackson ImmunoResearch, 1:400) for 1 h at room temperature and then stained with DAPI (Invitrogen) for 20 min. Whole mount sections were obtained via Z-stack reconstruction using the Leica SP8. For quantification, a region of interest defining the cytoplasm was determined by the DAPI and phalloidin staining for each cell. The average fluorescent intensity was calculated for the defined regions of interest. The labeling indices of Ki67, γ H2AX, CDX2, and SOX2 were calculated as the percentage (%) of positive nuclei among the total number of nuclei in each compartment.

H&E staining

Gastric organoids were fixed in 4% paraformaldehyde for 24 h at room temperature. The fixed organoids were subjected to H&E staining and alcian blue staining. Images were acquired using an Olympus IX73 Microscope System (Olympus Corporation).

IHC staining

For IHC staining, sections were first deparaffinized in xylene and rehydrated through a graded series of ethanol. The sectioned samples underwent IHC staining according to the manufacturer's instructions (ZSGB-BIO).

EdU labeling

To determine the rate of organoid proliferation, EdU staining was performed using a commercially available kit (C0071S, Beyotime Biotechnology) following the manufacturer's protocol. During the last 60 min of incubation, 20 μM EdU was added to the culture medium. Organoids were then fixed in 4% paraformaldehyde. EdU incorporation was visualized using a click reaction with Alexa Fluor® 488 Azide for detection. Nuclei were counterstained with Hoechst for 10 min. The ratio of EdU+cells to total cells was calculated by counting the respective nuclei.

Apoptosis assay

Organoids were stained with 10 μ g/ml propidium iodide (Thermo Scientific, P3566) to visualize dying cells and analyzed using fluorescence microscopy. The propidium iodide-positive area was quantified using ImageJ and compared between DMSO-treated and MNNG-treated organoids.

Acridine orange experiment

To assess the intracellular pH changes, organoids were incubated with acridine orange (1 μ M) for 15 min at 37°C and 5% CO $_2$. Fluorescence was excited at 488 nm, and images were captured in a time series at 600–650 nm or 500–550 nm. At each time point, a set of 10 x-y plane images was taken at 6 μ m focus intervals. Histamine (final concentration 100 μ M) was added to induce pH changes. The background-corrected F488 fluorescence ratio image was normalized to the histamine pretreatment baseline. pH values were calculated from the 600–650 nm/500–550 nm ratio using a previously established standard curve (Chu and Montrose, 1995; Schumacher et al., 2015).

Western blotting analysis

Total protein was extracted from cells that were homogenized in RIPA lysis buffer (Beyotime) containing proteinase and phosphatase inhibitors (Roche) and then centrifuged. Western blots were performed as previously described (Pillai-Kastoori et al., 2020). Image Lab software was used for densitometric analysis to measure the expression level of the target protein relative to the control (β -actin).

RNA-seq analysis

RNA isolation was performed using the RNeasy Mini Kit (Qiagen) following the manufacturer's instructions. After demultiplexing, reads for samples were processed using SAMtools (v1.4) (Li et al., 2009) and aligned using the splice aware aligner Hisat2 (v2.0.4) (Kim et al., 2015) with default parameters. The coordinates and gene annotations used for all subsequent analyses were based on the mouse genome assembly (mm10/GRCm38) and the corresponding UCSC RefSeq genes, unless otherwise specified.

Pathway enrichment analysis

GSEA was performed on differentially expressed genes (DEGs) in DM-GOs and MG-GOs. Reactome pathways from the MSigDB database (Subramanian et al., 2005) were used for data analysis, and the 'Intestinal metaplasia-related genes' pathway collections from the GSE78523 and GSE173624 were used for comparison. Mouse Gene Ontology terms were also used for GSEA data analysis (Luo et al., 2009; Korotkevich et al., 2021). Analysis was carried out using the R package fgsea, and the rank function was calculated as — log10(P-value) * log2(fold change). Pathway enrichments analysis was executed using 100000 permutations for P-value calculation.

Statistical analysis

All statistics are described in the figure legends. Statistical significance between two groups was determined using a two-tailed Student's *t*-test or Mann–Whitney test and that for more than two groups was determined using one-way analysis of variance (ANOVA) or two-way ANOVA with Bonferroni's multiple comparison test by GraphPad Prism 9.03 (GraphPad Software).

Supplementary material

Supplementary material is available at *Journal of Molecular Cell Biology* online.

Funding

This work was supported by grants from the National Natural Science Foundation of China (82205095, 82374292, 92059102, 32090040, 82204894, and 82305179), the China Postdoctoral Science Foundation (2022M720520), and the Anhui TCM Synergism Project (202303a0702003).

Conflict of interest: none declared.

References

- Aditi, A., and Graham, D.Y. (2012). Vitamin C, gastritis, and gastric disease: a historical review and update. Dig. Dis. Sci. *57*, 2504–2515.
- Babu, S.D., Jayanthi, V., Devaraj, N., et al. (2006). Expression profile of mucins (MUC2, MUC5AC and MUC6) in Helicobacter pylori infected pre-neoplastic and neoplastic human gastric epithelium. Mol. Cancer 5, 10.
- Barros, R., Freund, J.N., David, L., et al. (2012). Gastric intestinal metaplasia revisited: function and regulation of CDX2. Trends Mol. Med. 18, 555– 563.
- Bartfeld, S., Bayram, T., van de Wetering, M., et al. (2015). In vitro expansion of human gastric epithelial stem cells and their responses to bacterial infection. Gastroenterology 148, 126–136.e6.
- Bhat, A.A., Uppada, S., Achkar, I.W., et al. (2018). Tight junction proteins and signaling pathways in cancer and inflammation: a functional crosstalk. Front. Physiol. *9*, 1942.
- Bray, F., Ferlay, J., Soerjomataram, I., et al. (2018). Global cancer statistics 2018: GLOBOCAN estimates of incidence and mortality worldwide for 36 cancers in 185 countries. CA Cancer J. Clin. 68, 394–424.
- Burma, S., Chen, B.P., Murphy, M., et al. (2001). ATM phosphorylates histone H2AX in response to DNA double-strand breaks. J. Biol. Chem. 276, 42462–42467.
- Caldwell, B., Meyer, A.R., Weis, J.A., et al. (2022). Chief cell plasticity is the origin of metaplasia following acute injury in the stomach mucosa. Gut 71, 1068–1077.

- Camilo, V., Garrido, M., Valente, P., et al. (2015). Differentiation reprogramming in gastric intestinal metaplasia and dysplasia: role of SOX2 and CDX2. Histopathology *66*, 343–350.
- Chu, S., and Montrose, M.H. (1995). Extracellular pH regulation in microdomains of colonic crypts: effects of short-chain fatty acids. Proc. Natl Acad. Sci. USA 92, 3303–3307.
- Companioni, O., Sanz-Anquela, J.M., Pardo, M.L., et al. (2017). Gene expression study and pathway analysis of histological subtypes of intestinal metaplasia that progress to gastric cancer. PLoS One *12*, e0176043.
- Correa, P. (1992). Human gastric carcinogenesis: a multistep and multifactorial process—First American Cancer Society Award Lecture on Cancer Epidemiology and Prevention. Cancer Res. *52*, 6735–6740.
- Correa, P., Piazuelo, M.B., and Wilson, K.T. (2010). Pathology of gastric intestinal metaplasia: clinical implications. Am. J. Gastroenterol. *105*, 493–498.
- Fatehullah, A., Appleton, P.L., and Nathke, I.S. (2013). Cell and tissue polarity in the intestinal tract during tumourigenesis: cells still know the right way up, but tissue organization is lost. Philos. Trans. R. Soc. Lond. B Biol. Sci. *368*, 20130014.
- Francis, R., Guo, H., Streutker, C., et al. (2019). Gastrointestinal transcription factors drive lineage-specific developmental programs in organ specification and cancer. Sci. Adv. 5, eaax8898.
- Fujiwara-Tani, R., Okamoto, A., Katsuragawa, H., et al. (2021). BRAF mutation is associated with hyperplastic polyp-associated gastric cancer. Int. J. Mol. Sci. 22, 12724.
- Gonzalez, C.A., Sanz-Anquela, J.M., Gisbert, J.P., et al. (2013). Utility of subtyping intestinal metaplasia as marker of gastric cancer risk. A review of the evidence. Int. J. Cancer 133, 1023–1032.
- Graham, D.Y., Rugge, M., and Genta, R.M. (2019). Diagnosis: gastric intestinal metaplasia—what to do next? Curr. Opin. Gastroenterol. *35*, 535–543.
- Hallin, J., Bowcut, V., Calinisan, A., et al. (2022). Anti-tumor efficacy of a potent and selective non-covalent KRAS(G12D) inhibitor. Nat. Med. 28, 2171–2182.
- Hayakawa, Y., Ariyama, H., Stancikova, J., et al. (2015). Mist1 expressing gastric stem cells maintain the normal and neoplastic gastric epithelium and are supported by a perivascular stem cell niche. Cancer Cell 28, 800–
- Hayakawa, Y., Fox, J.G., and Wang, T.C. (2017). Isthmus stem cells are the origins of metaplasia in the gastric corpus. Cell. Mol. Gastroenterol. Hepatol. 4, 89–94.
- Higashi, H., Nakaya, A., Tsutsumi, R., et al. (2004). Helicobacter pylori CagA induces Ras-independent morphogenetic response through SHP-2 recruitment and activation. J. Biol. Chem. *279*, 17205–17216.
- Jiao, S., Wang, H., Shi, Z., et al. (2014). A peptide mimicking VGLL4 function acts as a YAP antagonist therapy against gastric cancer. Cancer Cell 25, 166–180.
- Johnson, T.E., Lee, J.H., Myler, L.R., et al. (2018). Homeodomain proteins directly regulate ATM kinase activity. Cell Rep. 24, 1471–1483.
- Kim, D., Langmead, B., and Salzberg, S.L. (2015). HISAT: a fast spliced aligner with low memory requirements. Nat. Methods 12, 357–360.
- Koide, T., Koyanagi-Aoi, M., Uehara, K., et al. (2022). CDX2-induced intestinal metaplasia in human gastric organoids derived from induced pluripotent stem cells. iScience 25, 104314.
- Korotkevich, G., Sukhov, V., Budin, N., et al. (2021). Fast gene set enrichment analysis. bioRxiv, https://doi.org/10.1101/060012
- Krishnan, V., Lim, D.X.E., Hoang, P.M., et al. (2020). DNA damage signalling as an anti-cancer barrier in gastric intestinal metaplasia. Gut *69*, 1738–1749.
- Lambrecht, N.W., Yakubov, I., Scott, D., et al. (2005). Identification of the K efflux channel coupled to the gastric H-K-ATPase during acid secretion. Physiol. Genomics *21*, 81–91.
- Lee, S.H., Lee, J.W., Soung, Y.H., et al. (2003). BRAF and KRAS mutations in stomach cancer. Oncogene 22, 6942–6945.
- Li, H., Handsaker, B., Wysoker, A., et al. (2009). The sequence alignment/map format and SAMtools. Bioinformatics *25*, 2078–2079.
- Li, J.S.Z., Abbasi, A., Kim, D.H., et al. (2023). Chromosomal fragile site breakage by EBV-encoded EBNA1 at clustered repeats. Nature *616*, 504–

- Liu, X., Xu, L., Li, J., et al. (2020). Mitotic motor CENP-E cooperates with PRC1 in temporal control of central spindle assembly. J. Mol. Cell Biol. 12, 654–665.
- Luo, W., Friedman, M.S., Shedden, K., et al. (2009). GAGE: generally applicable gene set enrichment for pathway analysis. BMC Bioinformatics 10, 161
- Mari, L., Milano, F., Parikh, K., et al. (2014). A pSMAD/CDX2 complex is essential for the intestinalization of epithelial metaplasia. Cell Rep. 7, 1197–1210.
- Matkar, S.S., Durham, A., Brice, A., et al. (2011). Systemic activation of K-ras rapidly induces gastric hyperplasia and metaplasia in mice. Am. J. Cancer. Res. 1. 432–445.
- Mesquita, P., Jonckheere, N., Almeida, R., et al. (2003). Human MUC2 mucin gene is transcriptionally regulated by Cdx homeodomain proteins in gastrointestinal carcinoma cell lines. J. Biol. Chem. 278, 51549-51556.
- Mills, J.C., and Goldenring, J.R. (2017). Metaplasia in the stomach arises from gastric chief cells. Cell. Mol. Gastroenterol. Hepatol. 4, 85–88.
- Narayanan, V., Purkayastha, P., Yu, B., et al. (2023). Rho activation drives luminal collapse and eversion in epithelial acini. Biophys. J. *122*, 3630–3645.
- Niwa, T., Ikehara, Y., Nakanishi, H., et al. (2005). Mixed gastric- and intestinaltype metaplasia is formed by cells with dual intestinal and gastric differentiation. J. Histochem. Cytochem. 53, 75–85.
- Olivieri, M., Cho, T., Alvarez-Quilon, A., et al. (2020). A genetic map of the response to DNA damage in human cells. Cell *182*, 481–496.e21.
- Ollivier, A., Mahe, M.M., and Guasch, G. (2021). Modeling gastrointestinal diseases using organoids to understand healing and regenerative processes. Cells 10, 1331.
- Ootani, A., Toda, S., Fujimoto, K., et al. (2000). An air-liquid interface promotes the differentiation of gastric surface mucous cells (GSM06) in culture. Biochem. Biophys. Res. Commun. *271*, 741–746.
- Owen, R.P., White, M.J., Severson, D.T., et al. (2018). Single cell RNA-seq reveals profound transcriptional similarity between Barrett's oesophagus and oesophageal submucosal glands. Nat. Commun. *9*, 4261.
- Park, D.Y., Srivastava, A., Kim, G.H., et al. (2010). CDX2 expression in the intestinal-type gastric epithelial neoplasia: frequency and significance. Mod. Pathol. 23, 54–61.
- Pillai-Kastoori, L., Schutz-Geschwender, A.R., and Harford, J.A. (2020). A systematic approach to quantitative western blot analysis. Anal. Biochem. 593, 113608.
- Rubin, E., Wu, X., Zhu, T., et al. (2007). A role for the HOXB7 homeodomain protein in DNA repair. Cancer Res. 67, 1527–1535.

- Schumacher, M.A., Aihara, E., Feng, R., et al. (2015). The use of murinederived fundic organoids in studies of gastric physiology. J. Physiol. *593*, 1809–1827.
- Shimizu, T., Choi, E., Petersen, C.P., et al. (2016). Characterization of progressive metaplasia in the gastric corpus mucosa of Mongolian gerbils infected with Helicobacter pylori. J. Pathol. 239, 399–410.
- Simmini, S., Bialecka, M., Huch, M., et al. (2014). Transformation of intestinal stem cells into gastric stem cells on loss of transcription factor Cdx2. Nat. Commun. 5, 5728.
- Smyth, E.C., Nilsson, M., Grabsch, H.I., et al. (2020). Gastric cancer. Lancet 396, 635–648.
- Song, X., Yang, F., Liu, X., et al. (2021). Dynamic crotonylation of EB1 by TIP60 ensures accurate spindle positioning in mitosis. Nat. Chem. Biol. 17, 1314–1323.
- Subramanian, A., Tamayo, P., Mootha, V.K., et al. (2005). Gene set enrichment analysis: a knowledge-based approach for interpreting genome-wide expression profiles. Proc. Natl Acad. Sci. USA 102, 15545–15550.
- Tang, Y., Fang, G., Guo, F., et al. (2020). Selective inhibition of STRN3containing PP2A phosphatase restores hippo tumor-suppressor activity in gastric cancer. Cancer Cell 38, 115–128.e9.
- Vermezovic, J., Stergiou, L., Hengartner, M.O., et al. (2012). Differential regulation of DNA damage response activation between somatic and germline cells in Caenorhabditis elegans. Cell Death Differ. 19, 1847–1855.
- Wang, F., Xia, P., Wu, F., et al. (2008). Helicobacter pylori VacA disrupts apical membrane-cytoskeletal interactions in gastric parietal cells. J. Biol. Chem. 283, 26714–26725.
- Wang, T., Ong, C.W., Shi, J., et al. (2011). Sequential expression of putative stem cell markers in gastric carcinogenesis. Br. J. Cancer 105, 658–665.
- Yamamoto, H., Bai, Y.Q., and Yuasa, Y. (2003). Homeodomain protein CDX2 regulates goblet-specific MUC2 gene expression. Biochem. Biophys. Res. Commun. 300. 813–818.
- Yao, X., and Smolka, A.J. (2019). Gastric parietal cell physiology and Helicobacter pylori-induced disease. Gastroenterology 156, 2158–2173.
- Zhu, G., Pei, L., Xia, H., et al. (2021). Role of oncogenic KRAS in the prognosis, diagnosis and treatment of colorectal cancer. Mol. Cancer *20*, 143.
- Zhu, Y., Zhou, J., Xia, H., et al. (2014). The Rho GTPase RhoE is a p53-regulated candidate tumor suppressor in cancer cells. Int. J. Oncol. 44, 896–904.
- Zhuo, W., Liu, Y., Li, S., et al. (2019). Long noncoding RNA GMAN, up-regulated in gastric cancer tissues, is associated with metastasis in patients and promotes translation of Ephrin A1 by competitively binding GMAN-AS. Gastroenterology 156, 676–691.e11.